Electronic structure and x-ray magnetic circular dichroism in Cu_3Au-type transition metal platinum alloys

V. N. Antonov* and B. N. Harmon
Ames Laboratory, Iowa State University, Ames, Iowa 50011

A. N. Yaresko
Max Planck Institute for Physics of Complex Systems, D-01187 Dresden, Germany

(Received 28 November 2000; revised manuscript received 20 February 2001; published 11 June 2001)

The electronic structure and x-ray magnetic circular dichroism (XMCD) in $X\mathrm{Pt}_3$ ($X=$ V, Cr, Mn, Fe, Co, Ni) and $X_3\mathrm{Pt}$ ($X=$ Fe, Co, Ni) compounds are investigated theoretically from first principles, using the fully relativistic Dirac LMTO band structure method. The electronic structure is obtained with the local spin-density approximation (LSDA). Theoretically calculated spin and orbital magnetic moments are found to be in good agreement with neutron and XMCD experimental data. An interpretation for systematic trends seen in the orbital and spin magnetic moments of the series $X\mathrm{Pt}_3$ is presented by analyzing the calculated spin- and orbital-projected density of d states. The important role of hybridization between the $3d$ transition metal and Pt d states in the formation of the orbital magnetic moments at the Pt site is emphasized. The x-ray absorption spectra as well as the x-ray circular magnetic dichroism at the K, $L_{2,3}$, and $M_{2,3}$ edges for transition metal sites and $L_{2,3}$, $M_{2,3}$, $M_{4,5}$, $N_{2,3}$, $N_{4,5}$, $N_{6,7}$, and $O_{2,3}$ edges for Pt sites are calculated for all nine compounds. Good agreement between theory and the experiment is obtained. The XMCD sum rules are used to compute the spin and orbital magnetic moments and the results are compared to the direct calculations.

DOI: 10.1103/PhysRevB.64.024402 PACS number(s): 71.28.+d, 75.30.Mb

I. INTRODUCTION

In recent years the investigation of magneto-optical effects in the soft x-ray range has gained great importance as a tool for the investigation of magnetic materials.[1] In 1975 the theoretical work of Erskine and Stern showed that the x-ray absorption could be used to determine the x-ray magnetic circular dichroism (XMCD) in transition metals when left- and right-circularly polarized x-ray beams are used.[2] In 1985 Thole *et al.*[3] predicted a strong magnetic dichroism in the $M_{4,5}$ x-ray absorption spectra of magnetic rare-earth materials (MXD), for which they calculated the temperature and polarization dependence. A year later this MXD effect was confirmed experimentally by van der Laan *et al.*[4] at the Tb $M_{4,5}$-absorption edge of terbium iron garnet. The next year Schütz *et al.*[5] performed measurements using x-ray transition at the K edge of iron with circularly polarized x rays, where the asymmetry in absorption was found to be of the order of 10^{-4}. This was shortly followed by the observation of magnetic extended x-ray absorption fine structure (EXAFS).[6] A theoretical description for the XMCD at the Fe K-absorption edge was given by Ebert *et al.*[7] using a spin-polarized version of relativistic multiple scattering theory. In 1990 Chen *et al.*[8] observed a large magnetic dichroism at the $L_{2,3}$ edge of nickel metal. Also cobalt and iron showed huge effects, which rapidly brought forward the study of magnetic $3d$ transition metals, which are of technological interest. Full multiplet calculations for $3d$ transition metal $L_{2,3}$ edges by Thole and van der Laan[9] were confirmed by several measurements on transition metal oxides. First considered as a rather exotic technique, MXD has now developed as an important measurement technique for local magnetic moments. XMCD enables a quantitative determination of spin and orbital magnetic moments,[10] element-specific imaging of magnetic domains,[11] or polarization analysis.[12]

Motivated by the developing interest in obtaining element specific magnetic moment information provided by XMCD measurements, we have calculated the electronic and magnetic structure for the important series of magnetic $3d$-transition metal platinum alloys and evaluated the theoretical XMCD spectra within the local spin density approximation. For these materials for which experiments have been performed, there is good agreement between our calculated spectra and experimental data. By analyzing our results across the series we are able to make conclusions about the so called XMCD sum rules for spin and orbital moments. In the rest of the introduction we describe the materials and previous studies. Section II gives details of the computational method, while Sec. III contains our results and their comparison with the experiment. Finally, Sec. IV summarizes the results and contains conclusions.

$3d$ transition metals and Pt form binary alloys in a wide range of concentration ratios having various magnetic properties. At stoichiometric compositions the alloys usually order. When the transition metal (represented by X) is one of the elements among V through Ni, ordered XPt has the CuAuI-type (or $L1_0$) structure and $X\mathrm{Pt}_3$ and $X_3\mathrm{Pt}$ have the Cu_3Au-type (or $L2_1$) structure.[13,14] Among the Cu_3Au-type ordered alloys with $X=$V to Ni, ferromagnetism is found for $MnPt_3$,[15] Fe_3Pt,[16] $CoPt_3$,[17] and Ni_3Pt,[18] while $FePt_3$ exhibits antiferromagnetism with a (1/2,1/2,0) magnetic ordering vector. For VPt_3 and $CrPt_3$, it is widely believed that the magnetic moments on Pt sites align in an antiparallel direction to those on the $3d$ transition metal sites, forming a ferrimagnetic ordering.

Transition-metal alloys consisting of a ferromagnetic $3d$ element and Pt have drawn attention over the last years due

to their wide variety of magnetic properties. In these intermetallic compounds, the Pt sites have induced magnetic moments due to the hybridization with the transition metal spin-polarized $3d$ states. The contribution of the orbital moment to the total moment on the Pt sites is expected to be important because the Pt atom is so heavy (atomic number $Z=78$) that the spin-orbit coupling of the Pt $5d$ electrons is fairly large (coupling constant $\zeta_{5d}=0.5$ eV).

The electronic structure and magnetic properties of $X\mathrm{Pt}_3$ compounds have been investigated theoretically in Refs. 19–29. Recently, Maruyama *et al.* measured magnetic circular x-ray dichroism for CrPt_3, MnPt_3, CoPt_3, and ferromagnetic $\mathrm{Fe}_3\mathrm{Pt}$ and obtained an interesting variation in the orbital and spin magnetic moments on the Pt sites.[30,31] The spin magnetic moment of Pt in CrPt_3 almost vanishes and the orbital moment is about $-0.1\mu_B$, antiferromagnetically coupled with the Cr magnetic moment. On the other hand, the orbital moment of Pt in MnPt_3 vanishes almost completely and a small but positive spin component (of the order of $0.1\mu_B$ parallel to the transition metal moment) contributes to the Pt moment. In CoPt_3 and $\mathrm{Fe}_3\mathrm{Pt}$, the Pt orbital and spin components are positive and relatively larger (in the range 0.1 to $0.3\mu_B$). Magnetic circular dichroism in the x-ray absorption spectrum in the $2p$-$3d$ excitation region of the transition-metal element was also measured for ferromagnetic $\mathrm{Cu}_3\mathrm{Au}$-type alloys MnPt_3, $\mathrm{Fe}_3\mathrm{Pt}$, and CoPt_3 in Ref. 18. The x-ray magnetic circular dichroism and Faraday effect were studied in ordered and disordered $\mathrm{Fe}_3\mathrm{Pt}$ at K- and L_3-edges in Ref. 32. Angle dependent XMCD experiments have been performed at both Co and Pt $L_{2,3}$ edges in Ref. 33. The MCD spectrum of ferromagnetic CoPt_3 was observed in the photon energy range of 50 to 80 eV in Ref. 34. MCD spectrum in the Pt $N_{6,7}$ $(4f\rightarrow 5d)$ region shows very unusual features. This MCD spectral shape deviates significantly from the one expected by considering the conventional selection rule of the dipole transition. It was shown in the frame of the Anderson impurity model that the unusual line shape of the MCD is caused by a strong interference (Fano effect for resonant photoemission).

With the aim of undertaking a systematic investigation of the trends in the transition-metal-platinum alloys, we have investigated the electronic structure, spin and orbital magnetic moments and XMCD spectra of the series $X\mathrm{Pt}_3$, X = V, Cr, Mn, Fe, Co, Ni and $X_3\mathrm{Pt}$($X=$ Fe, Co, Ni). We calculated the XAS and XMCD spectra at K, $L_{2,3}$, and $M_{2,3}$ edges for transition metals and $L_{2,3}$, $M_{2,3}$, $M_{4,5}$, $N_{2,3}$, $N_{4,5}$, $N_{6,7}$, and $O_{2,3}$ edges at Pt sites. The theoretical results are compared with available experimental data and the XMCD sum rule spin and orbital magnetic moments are compared to the direct calculations in Sec. III.

II. THEORETICAL DESCRIPTION AND COMPUTATIONAL DETAILS

Magneto-optical effects refer to various changes in the polarization state of light upon interaction with materials possessing a net magnetic moment, including rotation of the plane of linearly polarized light (Faraday, Kerr rotation), and the complementary differential absorption of left and right circularly polarized light (circular dichroism). In the near visible spectral range these effects result from excitation of electrons in the conduction band. Near x-ray absorption edges, or resonances, magneto-optical effects can be enhanced by transitions from well-defined atomic core levels to transition symmetry selected valence states. There are at least two alternative formalisms for describing resonant soft x-ray MO properties. One uses the classical dielectric tensor.[35] Another uses the resonant atomic scattering factor including charge and magnetic contributions.[36,37] The equivalence of these two description (within dipole approximation) is demonstrated in Ref. 38.

For the polar Kerr magnetization geometry and a crystal of tetragonal symmetry, where both the fourfold axis and the magnetization **M** are perpendicular to the sample surface and the z axis is chosen to be parallel to them, the dielectric tensor is composed of the diagonal ε_{xx} and ε_{zz}, and the off-diagonal ε_{xy} component in the form

$$\boldsymbol{\varepsilon}=\begin{pmatrix} \varepsilon_{xx} & \varepsilon_{xy} & 0 \\ -\varepsilon_{xy} & \varepsilon_{xx} & 0 \\ 0 & 0 & \varepsilon_{zz} \end{pmatrix}. \tag{1}$$

A complete description of MO effects in this formalism is given by the four nonzero elements of the dielectric tensor or, equivalently, by the complex refractive index $n(\omega)$

$$n(\omega)\equiv\sqrt{\varepsilon(\omega)}=1-\delta(\omega)+i\beta(\omega) \tag{2}$$

for several normal modes corresponding to the propagation of pure polarization states along specific directions in the sample. The solution of Maxwell's equations yields these normal modes.[39] One of these modes is for circular components of opposite $(\pm)$ helicity with wave vector $\mathbf{h}\|\mathbf{M}$ having indexes

$$n_{\pm}=1-\delta_{\pm}+i\beta_{\pm}=\sqrt{\varepsilon_{xx}\pm i\varepsilon_{xy}}. \tag{3}$$

The two other cases are for linear polarization with $\mathbf{h}\perp\mathbf{M}$.[38] One has electric vector $\mathbf{E}\|\mathbf{M}$ and index $n_{\|}=1-\delta_{\|}+i\beta_{\|}=\sqrt{\varepsilon_{zz}}$. The other has $\mathbf{E}\perp\mathbf{M}$ and $n_{\perp}=1-\delta_{\perp}+i\beta_{\perp}=\sqrt{(\varepsilon_{xx}^2+\varepsilon_{xy}^2)/\varepsilon_{xx}}$.

At normal light incidence the complex Faraday angle given by[38,40]

$$\phi_F(\omega)=\theta_F(\omega)-i\,\eta_F(\omega)=\frac{\omega l}{2c}(n_+-n_-), \tag{4}$$

where c is the speed of light, $\theta_F(\omega)$ and $\eta_F(\omega)$ are the Faraday rotation and the ellipticity. The complex Faraday response describes the polarization changes to the incident linear polarization on propagation through the film of thickness l. (The incident linearly polarized light is a coherent superposition of two circularly waves of opposite helicity).

Magnetic circular dichroism is first order in M (or ε_{xy}) and is given by $\beta_+-\beta_-$ or $\delta_+-\delta_-$, respectively, the later representing the magneto-optical rotation (MOR) of the plane of polarization (Faraday effect). Magnetic linear dichroism (MLD) $n_{\perp}-n_{\|}$ (also known as the Voigt effect) is quadratic in M. The Voigt effect is present in both ferromag-

nets and antiferromagnets, while the first order MO effects in the forward scattering beam are absent with the net magnetization in antiferromagnets.

The alternative consideration of the MO effects is based on the atomic scattering factor $f(\omega,q)$, which provides a microscopic description of the interaction of x-ray photons with magnetic ions. For forward scattering $(q=0)$ $f(\omega)=Z+f'(\omega)+if''(\omega)$, where Z is the atomic number. $f'(\omega)$ and $f''(\omega)$ are the anomalous dispersion corrections related to each other by the Kramers-Kronig transformation. The general equivalence of these two formalisms can be seen by noting the one-to-one correspondence of terms describing the same polarization dependence for the same normal modes.[38] For a multicomponent sample they relate to δ and β through

$$\delta(\omega)=\frac{2\pi c^2 r_e}{\omega^2}\sum_i Z_i f_i'(\omega)N_i, \tag{5}$$

$$\beta(\omega)=\frac{2\pi c^2 r_e}{\omega^2}\sum_i f_i''(\omega)N_i, \tag{6}$$

where the sum is over atomic spheres, each having number density N_i, and r_e is the classical electron radius. The x-ray absorption coefficient $\mu^{\lambda}(\omega)$ of polarization λ may be written in terms of the imaginary part of $f_{\lambda}(\omega)$ as

$$\mu^{\lambda}(\omega)=\frac{4\pi r_e c}{\Omega\omega}f_{\lambda}''(\omega), \tag{7}$$

where Ω is the atomic volume. X-ray MCD which is the difference in x-ray absorption for right- and left-circularly polarized photons $(\mu^+ - \mu^-)$ can be presented by $(f_+''-f_-'')$. Faraday rotation $\theta_F(\omega)$ of linear polarization measures MCD in the real part f_{λ}' of the resonant magnetic x-ray-scattering amplitude, i.e.,[41]

$$\theta_F(\omega)=\frac{\omega l}{2c}\mathrm{Re}[n_+-n_-]=\frac{\pi l r_e}{\Omega\omega}[f_-'(\omega)-f_+'(\omega)]. \tag{8}$$

Finally, the scattering x-ray intensity from an elemental magnet at the Bragg reflection measured in the resonant magnetic x-ray-scattering experiments is just the squared modulus of the total scattering amplitude, which is a linear combination of $(f_{\pm}'+if_{\pm}'', f_z'+if_z'')$ with the coefficients fully determined by the experimental geometry.[40] Multiple scattering theory is usually used to calculate the resonant magnetic x-ray scattering amplitude $(f'+if'')$.[35,40,42]

We should mentioned that the general equivalence of the dielectric tensor and scattering factor descriptions holds only in the case considering dipole transitions contributing to atomic scattering factor $f(\omega)$. Higher-order multipole terms have different polarization dependence.[36]

Using straightforward symmetry considerations it can be shown that all magneto-optical phenomena (XMCD, MO Kerr, and Faraday effects) is caused by the symmetry reduction, in comparison to the paramagnetic state, caused by magnetic ordering.[43] Concerning the XMCD properties this symmetry reduction only has consequences when SO coupling is considered in addition. Theoretical description of magnetic dichroism can be cast into four categories. On the one hand, there are one-particle (ground-state) and many-body (excited-state) theories; on the other hand, there are theories for single atoms and those which take into account the solid state. To name a few from each category, for atomic one-particle theories we refer to Refs. 44 and 45, for atomic many-particle multiplet theory to Refs. 46–49, for solid many-particle theories to Ref. 50, and for solid one-particle theories (photoelectron diffraction) to Refs. 51–54. A multiple-scattering approach to XMCD, a solid-state one-particle theory, has been proposed by Ebert *et al.*[55–57] and Tamura *et al.*[58]

To calculate the XMCD properties one has to account for magnetism and SO coupling at the same time when dealing with the electronic structure of the material considered. Performing corresponding band structure calculations, it is normally sufficient to treat SO coupling in a perturbative way. A more rigorous scheme, however, is obtained by starting from the Dirac equation set up in the framework of relativistic spin density functional theory.[59] There are quite a few band structure methods available now that are based on the Dirac equation.[60–62] In one of the schemes the basis functions are derived from the proper solution of the Dirac equation for the spin dependent single-site potentials.[63,64] In another one, the basis functions are obtained initially by solving the Dirac equation without the spin-dependent term and then this term is accounted for in the variational step.[63,65] In spite of this approximation, the latter scheme gives results in a close agreement with the former,[66] while being simpler to implement.

Within the one-particle approximation, the absorption coefficient μ for incident x-ray of polarization λ and photon energy $\hbar\omega$ can be determined as the probability of electron transition from an initial core state (with wave function ψ_j and energy E_j) to a final unoccupied state (with wave function $\psi_{n\mathbf{k}}$ and energy $E_{n\mathbf{k}}$)

$$\mu_j^{\lambda}(\omega)=\sum_{n\mathbf{k}}|\langle\Psi_{n\mathbf{k}}|\Pi_{\lambda}|\Psi_j\rangle|^2\delta(E_{n\mathbf{k}}-E_j-\hbar\omega)\,\theta(E_{n\mathbf{k}}-E_F). \tag{9}$$

The Π_{λ} is the dipole electron-photon interaction operator

$$\Pi_{\lambda}=-e\boldsymbol{\alpha}\mathbf{a}_{\lambda}, \tag{10}$$

where $\boldsymbol{\alpha}$ are the Dirac matrices, $\mathbf{a}_{\lambda}$ is the λ polarization unit vector of the photon potential vector $[a_{\pm}=1/\sqrt{2}(1,\pm i,0), a_z=(0,0,1)]$. (Here $+/-$ denotes, respectively, left and right circular photon polarizations with respect to the magnetization direction in the solid.) More detailed expressions of the matrix elements for the spin-polarized fully relativistic LMTO method may be found in Refs. 57,67.

While XMCD is calculated using Eq. (9), the main features can be understood already from a simplified expression for paramagnetic solids. With restriction to electric dipole transitions, keeping the integration only inside the atomic spheres (due to the highly localized core sates) and averaging with respect to polarization of the light one obtains the following expression for the absorption coefficient of the core level with (l,j) quantum numbers:[68]

$$\mu_{lj}^{0}(\omega)=\sum_{l',j'}\frac{2j+1}{4}\left(\frac{\delta_{l',l+1}\delta_{j',j+1}}{j+1}+\frac{\delta_{l',l-1}\delta_{j',j-1}}{j}+\frac{\delta_{l',l+1}\delta_{j',j}}{j(j+1)(2j+1)}\right)N_{l',j'}(E)C_{l,j}^{l',j'}(E), \quad (11)$$

where $N_{l',j'}(E)$ is the partial density of empty states and the $C_{l,j}^{l',j'}(E)$ radial matrix elements.[68]

Equation (11) allows only transitions with $\Delta l=\pm 1,\Delta j=0,\pm 1$ (dipole selection rules) which means that the absorption coefficient can be interpreted as a direct measure for the sum of (l,j)-resolved DOS curves weighed by the square of the corresponding radial matrix element (which usually is a smooth function of energy). This simple interpretation is also valid for the spin-polarized case.[35]

The details of the computational method are described in our previous paper,[69] and here we only mention several aspects. The electronic structure of the compounds was calculated self-consistently using the local spin density approximation[70] and the fully relativistic spin-polarized LMTO method in the atomic-sphere approximation, including the combined correction (ASA+CC).[63,60,62,65,71] Core-charge densities were recalculated at every iteration of the self-consistency loop. The basis consisted of the *s*, *p*, *d*, *f*, and *g* LMTO's at each site. The **k**-space integrations were performed with the improved tetrahedron method[72] and the self-consistent charge was obtained with 405 irreducible **k** points.

Finally, the intrinsic broadening mechanisms have been accounted for by folding XMCD spectra with a Lorentzian. For the finite lifetime of the core hole a constant width Γ_c, in general from Ref. 73, has been used. For the relaxation and other contributions of the excited electron an energy dependent width $\Gamma_V(E)$ according to the suggestion of Müller *et al.*[74] has been applied. The finite apparative resolution of the spectrometer has been accounted for by a Gaussian with a width of around 0.5 to 1 eV taken, as far as possible, from the literature.

III. RESULTS AND DISCUSSION

$X\mathrm{Pt}_3$ and $X_3\mathrm{Pt}$ compounds crystallize in the $\mathrm{Cu_3Au}$ type (or $L2_1$) crystal structure, the space group No. 221. In our band structure calculations we used the experimentally measured lattice constants 3.87 Å for $\mathrm{VPt_3}$, 3.8735 Å for $\mathrm{CrPt_3}$, 3.89 Å for $\mathrm{MnPt_3}$, 3.864 Å for $\mathrm{FePt_3}$, 3.831 Å for $\mathrm{CoPt_3}$, 3.668 Å for $\mathrm{Co_3Pt}$, and 3.73 Å for $\mathrm{Fe_3Pt}$.[75] A ferromagnetically ordered state is assumed for all these intermetallics even including $\mathrm{FePt_3}$, which actually has antiferromagnetic order for the observed ground state.

A. Magnetic moments

Orbital and spin magnetic moments are determined by the interplay of hybridization, exchange, and Coulomb interactions, crystal-field, and spin-orbit coupling. Table I presents the calculated spin (M_s) and orbital (M_l) magnetic moments in $X\mathrm{Pt_3}$ and $X_3\mathrm{Pt}$ compounds. Our calculated results are in good agreement with those from the FLAPW calculations by Iwashita *et al.*[26] The variation in the spin and orbital magnetic moments calculated inside the $3d$ transition metal and Pt atomic spheres in the $X\mathrm{Pt_3}$ intermetallics is compared with the experimentally measured moments in Fig. 1. The magnetic moments of the $X\mathrm{Pt_3}$ alloys were studied experimentally through neutron-scattering experiments already years ago.[76,77] These experiments showed that $\mathrm{CoPt_3}$ and $\mathrm{MnPt_3}$ are ferromagnets, while $\mathrm{CrPt_3}$ and $\mathrm{VPt_3}$ are ferrimagnets, and $\mathrm{FePt_3}$ is an antiferromagnet. The calculated spin magnetic moments of $\mathrm{CoPt_3}$ and $\mathrm{MnPt_3}$ at the $3d$ site are in good

TABLE I. Calculated spin M_S and orbital M_L magnetic moments (in μ_B) of $X\mathrm{Pt_3}$ and $X_3\mathrm{Pt}$ compounds.

		X atom		Pt atom	
	X	M_S	M_L	M_S	M_L
$X\mathrm{Pt_3}$	V	1.3751	0.0141	-0.0509	-0.0276
	Cr	2.6799	0.1789	-0.0300	-0.0558
	Mn	3.6985	0.0239	0.1244	-0.0014
	Fe	3.1370	0.1004	0.3045	0.0534
	Co	1.7079	0.0401	0.2384	0.0486
	Ni	0.4379	-0.0770	0.0780	0.0305
$X_3\mathrm{Pt}$	Fe	2.5062	0.0870	0.2889	0.0522
	Co	1.6379	0.0786	0.3153	0.0687
	Ni	0.5178	0.0198	0.2343	0.0866

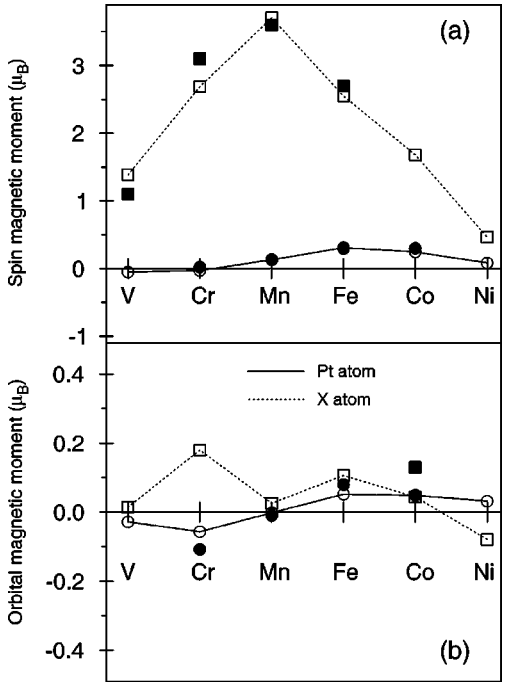

FIG. 1. Theoretically calculated spin (a) and orbital (b) magnetic moments on the Pt sites (open circles) and *X* sites (open squares) in comparison with the experimental data for $X\mathrm{Pt_3}$ and $\mathrm{Fe_3Pt}$ compounds. The experimental Pt orbital moments (solid circles) for $X=$ Cr, Mn, and Fe are from Ref. 31, Co orbital (solid square) and Pt orbital for $\mathrm{CoPt_3}$ are from Ref. 33, the experimental spin magnetic moments on *X* sites (solid squares) are from Ref. 76 and on Pt sites (solid circles) from Ref. 77.

agreement with the experiment, and for $CrPt_3$ and VPt_3 the ferrimagnetic structure is in accordance with experiment, but the values of the moments are less accurately reproduced. Due to band filling, linear and symmetric behavior centered at $MnPt_3$ is clearly seen in the spin magnetic moments on the $3d$ transition metal sites [Fig. 1(a)].

The characteristic feature of the electronic structure of XPt_3 compounds is the strong hybridization of transition metal $3d$ and Pt $5d$ states, the later being much more delocalized. Figure 2 shows the spin- and site-projected densities of the electronic states (DOS) for the transition metal site and the Pt site in XPt_3 compounds. Strong spin-orbit interaction in the Pt atomic sphere results in splitting of $d_{3/2}$ and $d_{5/2}$ states with the energy difference between their centers being $\sim$1.5 eV. Inside the X atomic spheres the effect of the spin-orbit coupling is much weaker than the effect of the exchange field. The centers of both Pt $d_{3/2}$ and $d_{5/2}$ states lie at lower energies than the centers of the corresponding X d states. As a result of the X d-Pt d hybridization, the electronic states at the bottom of the valence band are formed mainly by Pt states while the states in the vicinity of the Fermi level (E_F) have predominantly transition metal d character with an admixture of Pt d states. The hybridization with the exchange split X d states leads to a strong polarization of Pt d states near E_F. The resulting difference in occupation numbers for Pt states with the opposite spin projections gives rise to the appearance of a comparatively large spin magnetic moment at the Pt site. A large energy splitting between the spin-up and spin-down bands is found only for states with predominant $3d$ character. The minority-spin $3d$ states form rather narrow bands located near the top of the Pt d band in XPt_3 compounds. It is definitely seen in Fig. 2 that, as one proceeds from the lighter to heavier $3d$ elements, the spin-up $3d$ band is first filled up to $MnPt_3$ and then electrons start to occupy the spin-down $3d$ band. This explains the linear and symmetric behaviors in the spin moments of the $3d$ atoms mentioned above.

The Pt spin moment reflects hybridization of the Pt $5d$ states with the $3d$ bands. At the beginning of $3d$ series (VPt_3 and $CrPt_3$) and at the end ($NiPt_3$) the spin magnetic moment at Pt sites is very small. The spin-up $3d$ bands in $MnPt_3$, $FePt_3$, and $CoPt_3$ are nearly filled, therefore the spin-down hole in the Pt d states mixes with the empty $3d$ bands. Due to stronger hybridization between the Pt d states and the empty $3d$ bands in $FePt_3$ and $CoPt_3$ (Fig. 2) the Pt spin moments are larger than in $MnPt_3$ where the largest $3d$ moment was found. The agreement between calculated spin magnetic moments at Pt sites and the experimentally derived moments is very good [Fig. 1(a)].

As can be seen from Fig. 1(b) the variation in the orbital magnetic moments on the Pt sites observed by Maruyama *et al.* in XMCD experiments[31] is well reproduced by our calculations. However, the interpretation of the orbital moments is more complicated than in the case of the spin moments. To understand better the formation of Pt and $3d$ transition metal orbital magnetic moments let us introduce a site-dependent function $dm_{tl}(E)$ given by[78]

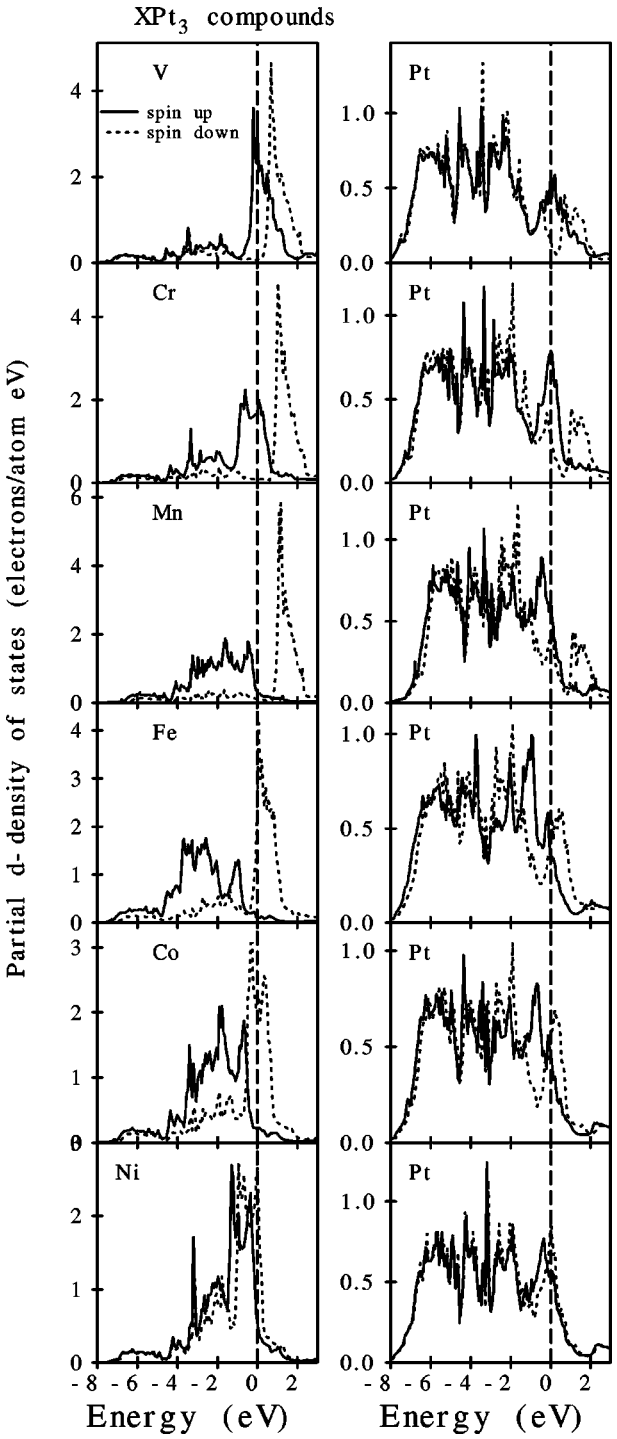

FIG. 2. Self-consistent fully relativistic, spin-polarized partial d-density of states of XPt_3 compounds (in electrons/atom eV).

$$dm_{tl}(E)=\sum_{n\mathbf{k}} \langle \Psi_{tl}^{n\mathbf{k}}|\hat{l}_z|\Psi_{tl}^{n\mathbf{k}}\rangle \delta(E-E_{n\mathbf{k}}), \qquad (12)$$

where $\hat{l}_z$ is z projection of the angular momentum operator, $E_{n\mathbf{k}}$ and $\Psi_{tl}^{n\mathbf{k}}$ are the energy of the nth band and the part of the corresponding LMTO wave function formed by the states with the angular momentum l inside the atomic sphere centered at the site t, respectively. In analogy to the l-projected

density of states, $dm_{tl}(E)$ can be referred to as site- and l-projected density of the expectation value of $\hat{l}_z$. This quantity has purely relativistic origins and when the SO interaction is equal to zero $dm_{tl}(E) \equiv 0$. As van Vleck[79] showed for a free ion, the absence of orbital degeneracy is a sufficient condition for the quenching of the orbital moment, which means that the first-order contribution should vanish: $\langle \Psi_{\mathbf{k}} | \hat{l}_z | \Psi_{\mathbf{k}} \rangle = 0$. Thus, $dm_{tl}(E)$ can be considered as the measure of unquenching of the orbital moment due to the SO interaction.

Furthermore, just as the number of states is defined as the integral of DOS, we can define the integral of $dm_{tl}(E)$

$$m_{tl}(E) = \int_{E_b}^{E} dm_{tl}(E) dE, \tag{13}$$

where E_b is the bottom of the valence band. Then, the orbital moment M_l at the site t is given by

$$M_l \equiv m_{tl}(E_F) \tag{14}$$

(here and henceforth we will drop the index t for simplicity).

Both $dm_l(E)$ and $m_l(E)$ are defined in the local coordinate system chosen in such a way that z axis is directed along the magnetization. It is worth noting that the only nonzero matrix elements of the $\hat{l}_z$ operator calculated between real harmonics with $l=2$ are $|\langle d_{x^2-y^2} | \hat{l}_z | d_{xy} \rangle| = 2$ and $|\langle d_{xz} | \hat{l}_z | d_{yz} \rangle| = 1$. Hence, the largest contribution to $m_l(E)$ can be expected from the $d_{x^2-y^2}$ and d_{xy} orbitals. The $m_l(E)$ function is proportional to the strength of the SO interaction and the value of the spin magnetic moment and it depends on the local symmetry. In the particular case of $X\mathrm{Pt}_3$ compounds the local symmetry for X atoms is O_h and for Pt atom it is D_{4h}. For the O_h group, basis functions are E_g (d_{z^2}, $d_{x^2-y^2}$) and T_{2g} (d_{xy}, d_{yz}, d_{xz}) while for the D_{4h} group they are A_{1g} (d_{z^2}), B_{1g} ($d_{x^2-y^2}$), B_{2g} (d_{xy}) and E_g (d_{yz}, d_{xz}). So the largest contribution to $m_l(E)$ can be expected in the case when we have simultaneously (at the same energy) a large contribution from the B_{1g} and B_{2g} states at Pt sites and the E_g and T_{2g} states at X sites in $X\mathrm{Pt}_3$ compounds.

Figure 3 shows the functions $dm_l(E)$ and $m_l(E)$ calculated for Co and Pt sites together with the partial d density of states in $CoPt_3$ as an example. Here and in the rest of the paper we will only consider the contribution coming from d orbitals to the m_l related functions. Both the $dm_l(E)$ and $m_l(E)$ functions show strong energy dependence. Although the variations of the functions at Co site are significantly larger in comparison with those at Pt sites, Pt and Co d orbital moments M_l are almost equal [see Fig. 1(b) and Table I].

When considering the $m_l(E)$ (Fig. 4) as well as $dm_l(E)$ (not shown) functions for $X\mathrm{Pt}_3$ compounds, one recognizes that especially those of VPt_3, $CrPt_3$, $MnPt_3$, $FePt_3$, and $CoPt_3$ are very similar for both the X and Pt sites respectively. In going from VPt_3 to $CoPt_3$ the Fermi level is simply shifted upwards by filling the bands with electrons. In $CrPt_3$ the Fermi level crosses $m_l(E)$ function at maximum and minimum at Cr and Pt sites, respectively, producing rather large Cr and Pt orbital moments with opposite sign [Fig. 1(b)

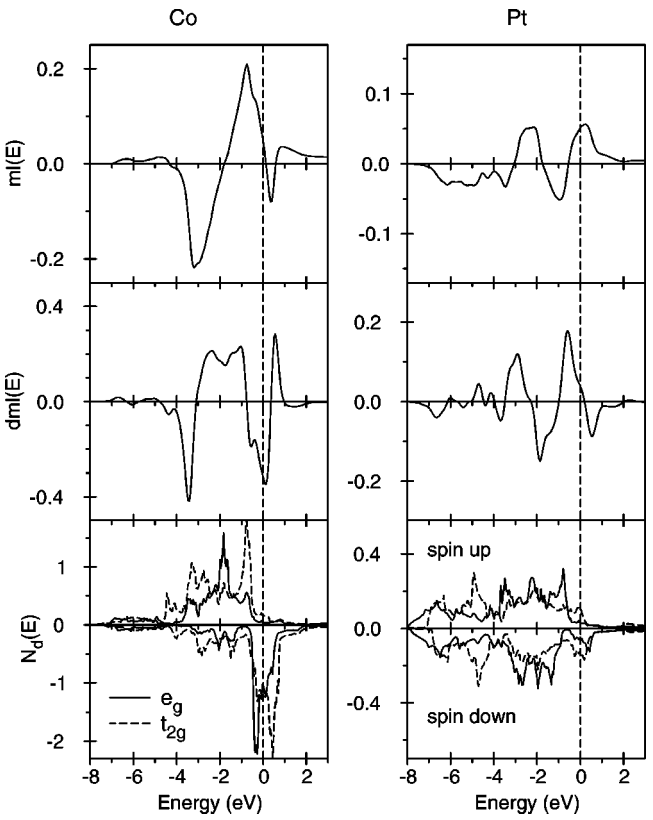

FIG. 3. The $dm_l(E)$, $m_l(E)$ functions and partial densities of states (in electrons/atom eV spin) for $l=2$ in $CoPt_3$.

and Table I]. In $MnPt_3$ due to filling the bands with one more electron, the Fermi level is situated at the local minimum in $m_l^{\mathrm{Mn}}(E)$ and at zero crossing in $m_l^{\mathrm{Pt}}(E)$. As a result $MnPt_3$ has a very small orbital magnetic moment at the Mn site and almost a zero Pt orbital moment. Further shifting of the Fermi level in $FePt_3$ places the Fermi level at a local maximum at both the Fe and Pt sites, providing rather large Fe and Pt orbital moments with the same sign. In $NiPt_3$ spin magnetic moment at Ni site is reduced substantially (see Table I), which correlates with the strong decrease of $m_2(E)$ at both the Ni and Pt sites. In addition, Ni $3d$ states are more localized in comparison with other $X\mathrm{Pt}_3$ compounds which manifests itself in weakening of the $3d$-$5d$ hybridization and can be a possible source of the noticeable change of the shape of $m_2(E)$ function at Pt site.

It is interesting to compare the electronic structure and orbital magnetic moments in the $X\mathrm{Pt}_3$ and $X_3\mathrm{Pt}$ compounds. Figure 5 shows d partial density of states in $CoPt_3$ and Co_3Pt compounds at both the Co and Pt sites. In the $CoPt_3$ compound the transition metal site is surrounded by 12 Pt sites. On the other hand, in Co_3Pt, four of the nearest neighbors are Pt sites and the other eight are Co sites. This difference in Co-Co coordination has a dramatic effect on the width of the $3d$ spin down DOS near the Fermi level. The $3d$ spin up states are centered more in the middle of the energy range of the Pt $5d$ states and therefore the Co orbitals hybridize rather effectively with the $5d$ orbitals in both the $CoPt_3$ and Co_3Pt compounds. On the other hand, $3d$ spin down states are centered in vicinity of the Fermi level where the Pt $5d$ DOS is

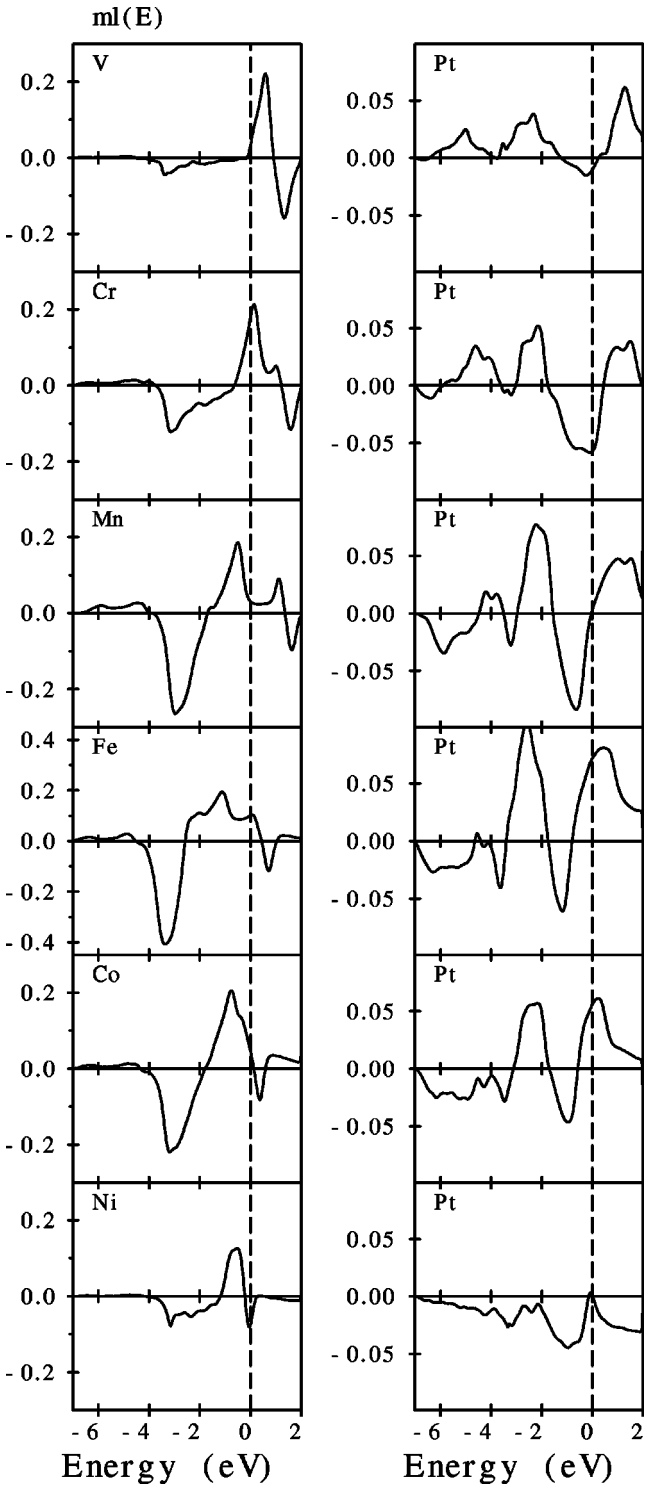

FIG. 4. The $m_l(E)$ functions for $l=2$ in $X\mathrm{Pt}_3$ compounds.

rather small. As a result they have smaller $3d$-$5d$ hybridization. Thus the $3d$ spin down states are more localized in $CoPt_3$ and more itinerant in Co_3Pt.

B. XMCD spectra

At the core level edge XMCD is not only element-specific but also orbital specific. For $3d$ transition metals, the electronic states can be probed by the K, $L_{2,3}$, and $M_{2,3}$ x-ray absorption and emission spectra whereas in $5d$ transition metals one can use the K, $L_{2,3}$, $M_{2,3}$, $M_{4,5}$, $N_{2,3}$, $N_{4,5}$, $N_{6,7}$, and $O_{2,3}$ spectra. As pointed out above, Eq. (11) for unpolarized absorption spectra $\mu^0(\omega)$ allows only transitions with $\Delta l=\pm 1, \Delta j=0,\pm 1$ (dipole selection rules). Therefore only electronic states with an appropriate symmetry contribute to the absorption and emission spectra under consideration (Table II). We should mention that in some cases quadrupole transitions may play an important role, as it occurs, for example, in rare earth materials ($2p\rightarrow 4f$ transitions).[80]

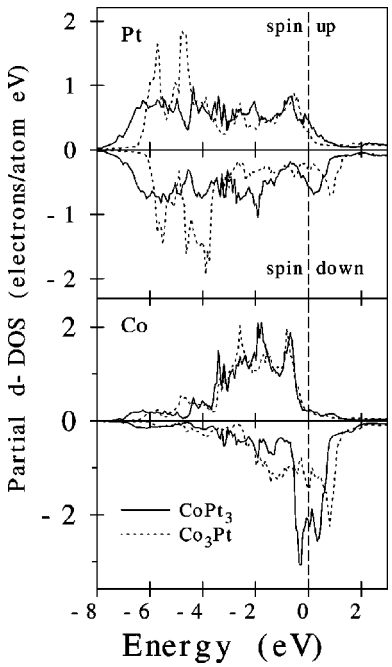

FIG. 5. Self-consistent fully relativistic, spin-polarized partial d-density of states of $CoPt_3$ and Co_3Pt compounds (in electrons/atom eV).

1. *K-edge of 3d-transition metal elements*

Figure 6 shows the theoretically calculated XMCD in terms of the difference in absorption $\Delta\mu_K=\mu_K^+-\mu_K^-$ for left

TABLE II. Angular momentum symmetry levels indicating the dipole allowed transitions from core states to the unoccupied valence states with the indicated partial density of states character.

Spectra	K	L_2 M_2 N_2 O_2	L_3 M_3 N_3 O_3	M_4 N_4	M_5 N_5	N_6	N_7
Core level	$1s_{1/2}$	$2p_{1/2}$ $3p_{1/2}$ $4p_{1/2}$ $5p_{1/2}$	$2p_{3/2}$ $3p_{3/2}$ $4p_{3/2}$ $5p_{3/2}$	$3d_{3/2}$ $4d_{3/2}$	$3d_{5/2}$ $4d_{5/2}$	$4f_{5/2}$	$4f_{7/2}$
Valence states	$p_{1/2}$ $p_{3/2}$	$s_{1/2}$ $d_{3/2}$	$s_{1/2}$ $d_{3/2}$ $d_{5/2}$	$p_{1/2}$ $p_{3/2}$ $f_{5/2}$	$p_{3/2}$ $f_{5/2}$ $f_{7/2}$	$d_{3/2}$ $d_{5/2}$ $g_{7/2}$	$d_{5/2}$ $g_{7/2}$ $g_{9/2}$

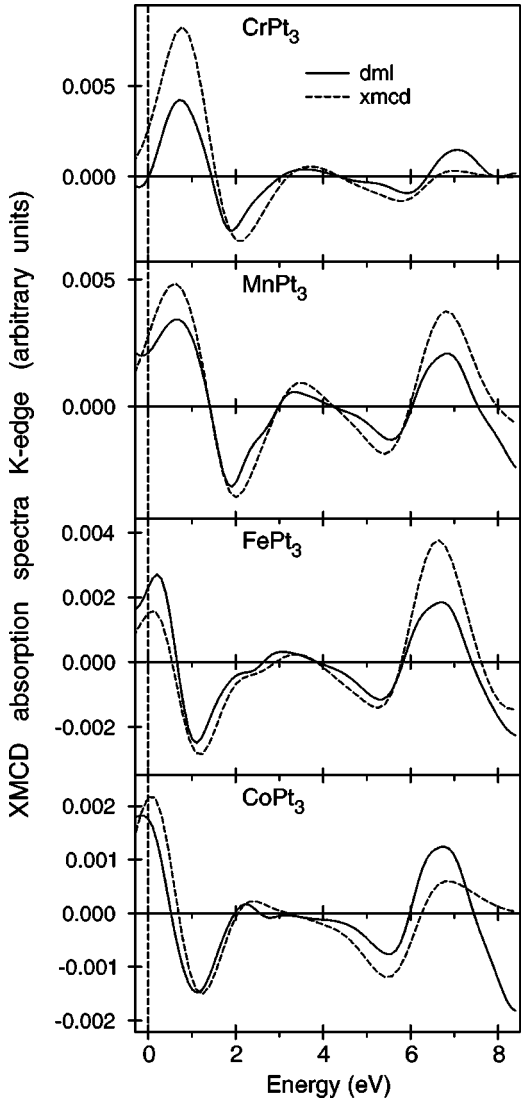

FIG. 6. Theoretically calculated $3d$ transition metal K-XMCD absorption spectra in comparison with $dm_{l=1}(E)$ function in $X\mathrm{Pt}_3$ alloys.

and right circularly polarized radiation in $X\mathrm{Pt}_3$ (X=Mn, Fe, and Co) compounds. Because dipole allowed transitions dominate the absorption spectrum for unpolarized radiation, the absorption coefficient $\mu_{\mathrm{K}}^0(E)$ (not shown) reflects primarily the DOS of unoccupied $4p$-like states $N_p(E)$ of X above the Fermi level. Due to the energy dependent radial matrix element for the $1s\rightarrow 4p$ there is no strict one-to-one correspondence between $\mu_{\mathrm{K}}(E)$ and $N_p(E)$. The exchange splitting of the initial $1s$-core state is extremely small[81] therefore only the exchange and spin-orbit splitting of the final $4p$ states is responsible for the observed dichroism at the K edge. For this reason the dichroism is found to be very small (Fig. 6). It was first pointed out by Gotsis and Strange[82] as well as Brooks and Johansson[83] that XMCD K spectrum reflects the orbital polarization in differential form $d\langle l_z\rangle/dE$ of the p states. As Fig. 6 demonstrates, where K XMCD spectra is shown together with $dm_{l=1}(E)$ functions [Eq. (12)], both quantities are indeed closely related to one another giving a rather simple and straightforward interpretation of the XMCD spectra at the K edge.

As in the case of absorption, K-emission XMCD spectrum (not shown) is in close relationship with site- and l-projected density of the expectation value of $\hat{l}_z$. Using the sum rule derived for K spectra in Ref. 84 we obtain a Mn $5p$ orbital magnetic moment of around $-0.0019\mu_{\mathrm{B}}$ in a good agreement with LSDA calculations ($-0.0016\mu_{\mathrm{B}}$).

2. $L_{2,3}$- and $M_{2,3}$-edges of 3d-transition metal elements

Because of the dipole selection rules, apart from the $4s_{1/2}$ states (which have a small contribution to the XAS due to relatively small $2p\rightarrow 4s$ matrix elements[35]) only $3d_{3/2}$ states occur as final states for L_2 XAS for unpolarized radiation, whereas for the L_3 XAS $3d_{5/2}$ states also contribute (Table II). Although the $2p_{3/2}\rightarrow 3d_{3/2}$ radial matrix elements are only slightly smaller than for the $2p_{3/2}\rightarrow 3d_{5/2}$ transitions the angular matrix elements strongly suppress the $2p_{3/2}\rightarrow 3d_{3/2}$ contribution [see Eq. (11)]. Therefore in neglecting the energy dependence of the radial matrix elements, the L_2 and the L_3 spectrum can be viewed as a direct mapping of the DOS curve for $3d_{3/2}$ and $3d_{5/2}$ character, respectively.

In contrast to the K edge, the dichroism at the L_2 and L_3 edges is also influenced by the spin-orbit coupling of the initial $2p$-core states. This gives rise to a very pronounced dichroism in comparison with the dichroism at the K edge. Figure 7 shows the theoretically calculated $3d$ transition metal $L_{2,3}$-XMCD spectra in $X\mathrm{Pt}_3$ alloys in comparison with the experimental data.[18] One finds that the theoretical XMCD spectra for the late transition metals to be in good agreement with experiment. For MnPt_3 the calculated magnetic dichroism is somewhat too high at the L_2 edge. As one can see, the XMCD spectra for $\mathrm{Fe}_3\mathrm{Pt}$, CoPt_3, and NiPt_3 are very similar with strong decreasing of the dichroism in NiPt_3 reflecting first of all the decrease of the spin magnetic moment in the later compound at the transition metal site (Table I). The XMCD spectra of ferrimagnetic VPt_3 and CrPt_3 differ significantly at the L_3 edge from the spectra of the ferromagnetic compounds. The former spectra have an additional positive peak in the low energy region.

The XMCD spectra at the $L_{2,3}$ edges are mostly determined by the strength of the SO coupling of the initial $2p$-core states and spin polarization of the final empty $3d_{3/2,5/2}$ states while the exchange splitting of the $2p$-core states as well as the SO coupling of the $3d$-valence states are of minor importance for the XMCD at the $L_{2,3}$ edge of $3d$-transition metals.[35]

To investigate the influence of the initial state on the resulting XMCD spectra we calculated also the XAS and XMCD spectra of $X\mathrm{Pt}_3$ compounds at the $M_{2,3}$ edge. The spin-orbit splitting of the $3p$-core level is of one order of magnitude smaller (from about 0.73 eV in V to 2.2 eV in Ni) than for the $2p$ level (from 7.7 eV in V to 17.3 eV in Ni) at the X site in the $X\mathrm{Pt}_3$ compounds. As a result the magnetic dichroism at the $M_{2,3}$ edge is much smaller than at the $L_{2,3}$ edge (Fig. 7). In addition, the M_2 and the M_3 spectra are strongly overlapped and the M_3 spectrum contributes to some extent to the structure of the total $M_{2,3}$ spectrum in the

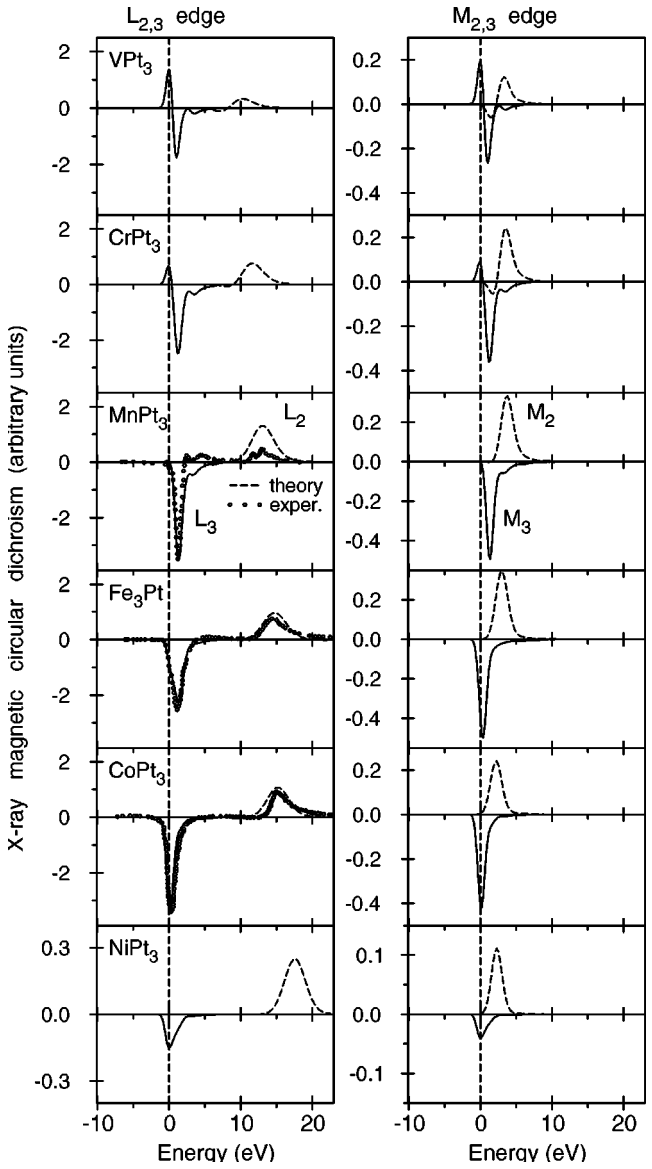

FIG. 7. Theoretically calculated $3d$ transition metal L_3 (full line), L_2 (dotted line), and M_3 (full line), M_2 (dotted line) XMCD spectra in $X\mathrm{Pt}_3$ alloys in comparison with available experimental data (circles) (Ref. 18).

region of the M_2 edge. To decompose a corresponding experimental $M_{2,3}$ spectrum into its M_2 and M_3 parts will therefore be quite difficult in general. It worth to mentioning that the shape of L_3 and M_3 XMCD spectra are very similar.

3. Pt $L_{2,3}$ edges

As mentioned above, MXCD investigations supply information on magnetic properties in a component resolved way. This seems especially interesting if there is a magnetic moment induced at a normally nonmagnetic element by neighboring magnetic atoms. The underlying mechanism of the magnetic and magneto-optical properties of the systems considered here is the well known ability of transition metals to induce large spin polarization of Pt via strong $3d$-$5d$ hybridization and exchange interaction. A very extreme example for this situation occurs for Pt in the $X\mathrm{Pt}_3$ compounds.

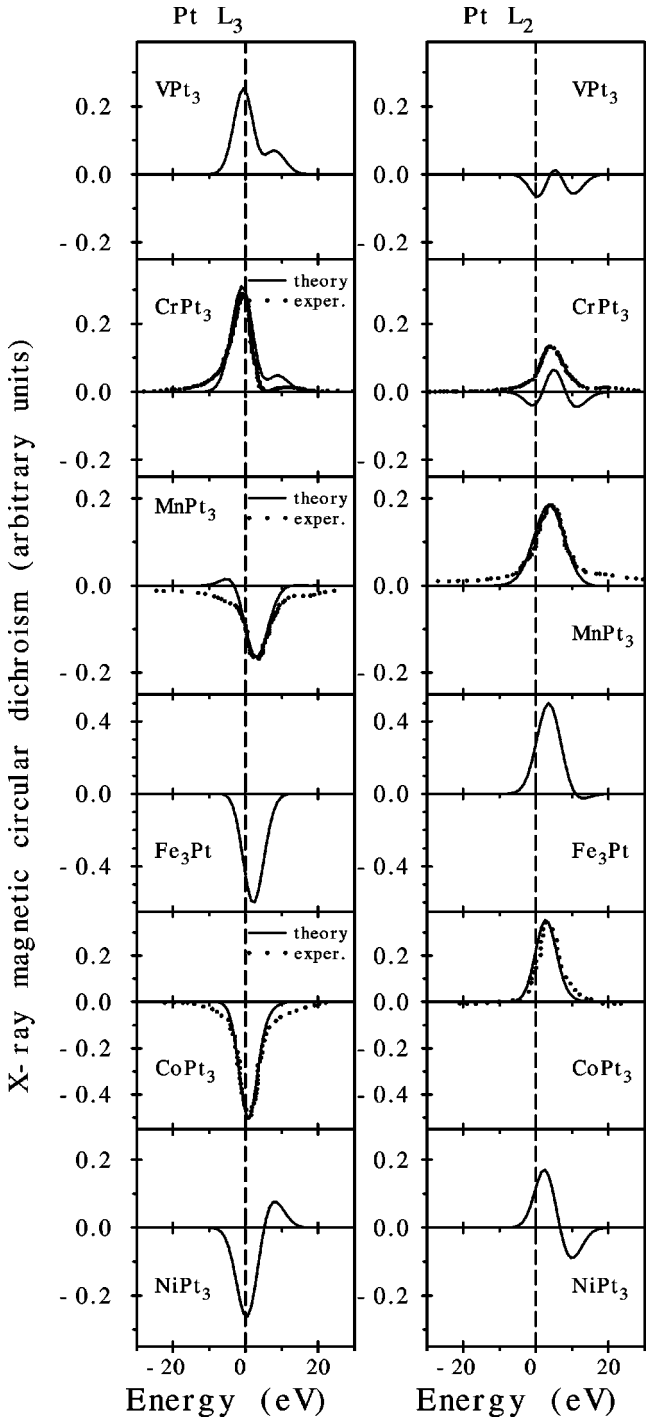

FIG. 8. Theoretically calculated Pt $L_{2,3}$ XMCD spectra in $X\mathrm{Pt}_3$ alloys (full line) in comparison with the experiment (circles), the experimental data for CrPt_3 are from Ref. 30, MnPt_3 from Ref. 31, and CoPt_3 from Ref. 33.

Results of the theoretical calculations for the circular dichroism at the $L_{2,3}$ edge of Pt are shown in Fig. 8 in comparison with the experimental data.[31,30] As one can see, a rather pronounced XMCD is found. In ferromagnetic compounds MnPt_3, $\mathrm{Fe}_3\mathrm{Pt}$, and CoPt_3, the XMCD spectrum is negative at the L_3 and positive at the L_2 edge as has been seen for the XMCD spectra at $L_{2,3}$ edges of the $3d$-transition

metals (Fig. 7). The XMCD in $MnPt_3$ at the L_3 and L_2 edges are of nearly equal magnitude, which suggest that an orbital magnetic moment almost vanishes in the Pt 5*d* states in this compound.[31] In ferromagnetically ordered VPt_3 and $CrPt_3$ the XMCD spectra at the L_3 edge are positive with a double peak structure in a good agreement with the experimental measurements.[30] The experimental XMCD spectrum of $CrPt_3$ at the Pt L_2 edge shows a positive sign although the theoretically calculated spectrum has additional negative components at both the low and high energy sides of the main peak (Fig. 8).

4. Pt M, N, and O edges

To investigate the influence of the initial state on the resulting Pt XMCD spectra we calculated also the XAS and XMCD spectra of XPt_3 compounds at the $M_{2,3}$, $M_{4,5}$, $N_{2,3}$, $N_{4,5}$, $N_{6,7}$, and $O_{2,3}$ edges. We found a systematic decreasing of the XMCD spectra in terms of $R=\Delta\mu/(2\mu_K^0)$ in the row $L_{2,3}$-$M_{2,3}$-$N_{2,3}$ edges. Although the magnetic dichroism of quasicore states ($O_{2,3}$ and $N_{6,7}$ edges) became almost as large as at the $L_{2,3}$ edge. In addition, the lifetime widths of the core $O_{2,3}$ and $N_{6,7}$ levels are much smaller than $L_{2,3}$ ones.[73] Therefore the spectroscopy of Pt atoms in the ultrasoft x-ray energy range at the $O_{2,3}$ and $N_{6,7}$ edges may be a very useful tool for investigating the electronic structure of magnetic materials.

Pt $M_{4,5}$ and $N_{4,5}$ spectra to some extent can be considered as an analog of the *K* spectrum. As it was mentioned above, *K* absorption spectrum at both sites reflects the energy distribution of empty $p_{1/2}$ and $p_{3/2}$ energy states (Table II). The M_4 (N_4) absorption spectra due to the dipole selection rules occur for the transition from the $3d_{3/2}$ ($4d_{3/2}$) core states to the $p_{1/2}$, $p_{3/2}$, and $f_{5/2}$ valence states above Fermi level, whereas for the M_5 (N_5) XAS the $p_{3/2}$, $f_{5/2}$, and $f_{7/2}$ states contributes. Results of the theoretical calculations of the circular dichroism in absorption at the $N_{4,5}$ edge of Pt in the XPt_3 ($X=$ Cr, Mn and Fe) are shown in Fig. 9. Comparing this spectra with the corresponding XMCD spectra of transition metals at the *K* edge (Fig. 6) one can see an obvious resemblance between these two quantities (the magnetic dichroism at the N_4 edge has an opposite sign to the XMCD at the *K* and N_5 edge). Such a resemblance reflects the similarity of the energy distribution of unoccupied *p* local partial densities of states $N_p(E)$ just above the Fermi level at *X* and Pt sites (not shown). It occurs due to a strong *X p*-Pt *p* hybridization effect. The major difference is seen at 0 to 2 eV. It can be attributed to an additional contribution of the $f_{5/2,7/2}$ energy states to the $N_{4,5}$ spectra and to the difference in the radial matrix elements ($1s\rightarrow p_{1/2,3/2}$ in *K* spectra and $4d_{3/2,5/2}\rightarrow p_{1/2,3/2}$ in $N_{4,5}$ spectra). Although the later plays a minor role due to the fact that radial matrix elements are smooth functions of energy.

It is interesting to compare Pt XAS and XMCD spectra at the $L_{2,3}$, $O_{2,3}$, and $N_{6,7}$ edges. Due to the dipole selection rules, for unpolarized radiation (apart from the $s_{1/2}$ states which have a small contribution to the XAS) only $3d_{3/2}$ states occur as final states for L_2 as well as for O_2 spectra (Table II). The L_3 and O_3 spectra reflect the energy distribution of both the $3d_{3/2}$ and $3d_{5/2}$ empty states. On the other hand, the N_7 absorption spectrum reflects only the $3d_{5/2}$ states (the density of the $g_{7/2,9/2}$ states is really very small) whereas for the N_6 XAS both the $3d_{3/2}$ and $3d_{5/2}$ states contribute. Therefore we have an inverse situation: N_6 absorption spectra correspond to the L_3 and O_3 spectra, whereas the N_7 is the analog of the L_2 and O_2 ones. This situation is clearly seen in Fig. 10 where the theoretically calculated XMCD spectra of XPt_3 compounds at the $O_{2,3}$ and $N_{6,7}$ edges is presented. The XMCD spectra at O_3 edges are almost identical to the spectra at the N_6 edges. The XMCD spectra at O_2 edges are also very similar to the spectra at the N_7 edges (but not identical because the energy distribution of Pt $3d_{3/2}$ and $3d_{3/2}$ states is not exactly the same due to SO interaction). The magnetic dichroism (e.g., in $CoPt_3$) is negative at the O_3 edge and positive at the O_2 edge (as it was at $L_{2,3}$ edges, see Fig. 8), but the XMCD is positive at the N_7 edge and negative at the N_6 one. However, we emphasize that O_3 (O_2) and N_6 (N_7) XMCD spectra are not identical to the L_3 (L_2) ones. One can argue that at least for Pt the $L_{2,3}$ spectra predominantly reflect atomic aspects of the valence band while for the $O_{2,3}$ and $N_{6,7}$ edge the itinerant aspects are more important. This is especially pronounced in ferrimagnetic VPt_3, $CrPt_3$ and ferromagnetic $MnPt_3$ with more itinerant character of the valence states than in $CoPt_3$ and $NiPt_3$ with relatively more localized $3d$ states.

Because of the relatively small spin-orbit splitting of the $4f$ states of Pt ($\sim$3.3 eV), the N_6 and the N_7 spectra have an appreciable overlap. For this reason the N_7 spectrum contributes to some extent to the structure of the total $N_{6,7}$ spectrum in the region of the N_6 edge, as can be seen from Fig. 10. To decompose a corresponding experimental $N_{6,7}$ spectrum into its N_6 and N_7 parts will therefore be quite difficult in general.

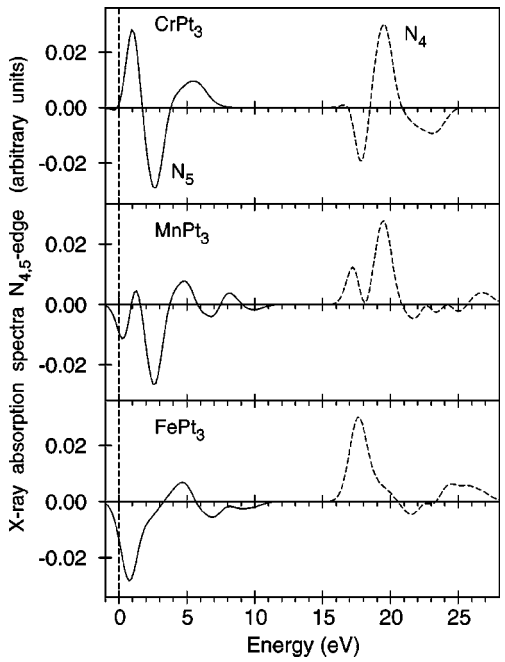

FIG. 9. Theoretically calculated Pt $N_{4,5}$ XMCD spectra in XPt_3 alloys.

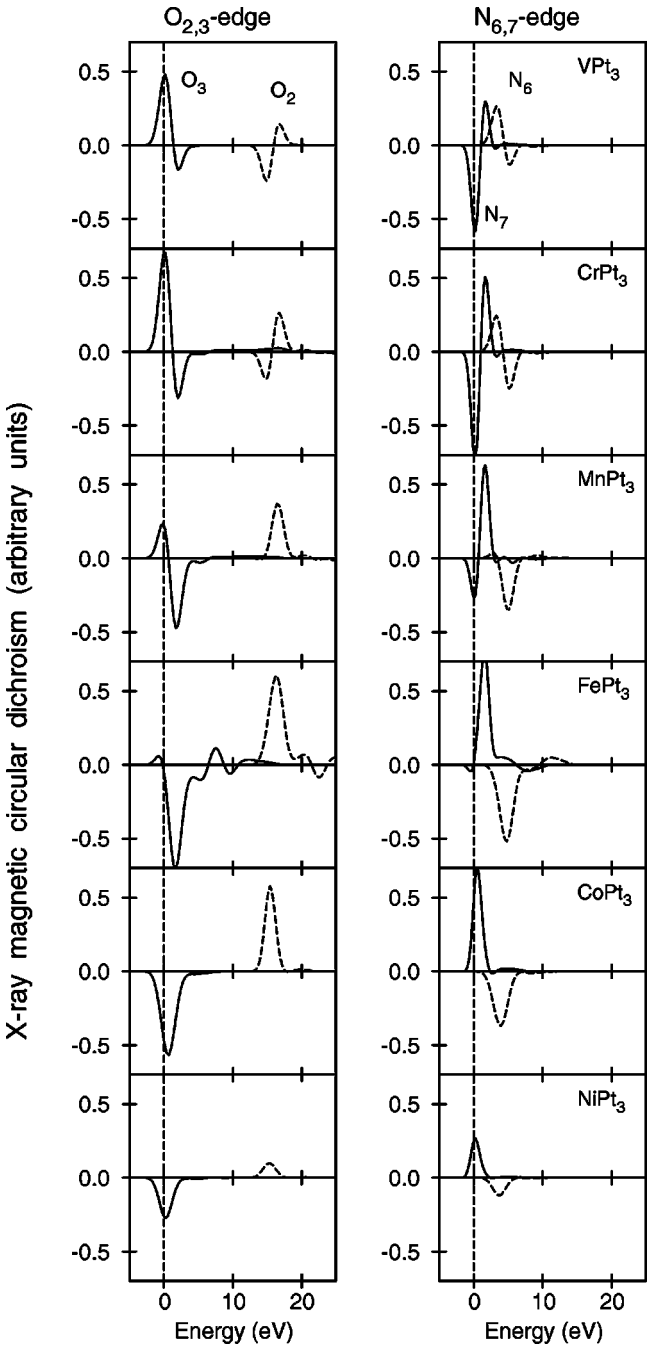

FIG. 10. Theoretically calculated Pt $O_{2,3}$ and $N_{6,7}$ XMCD spectra in XPt_3 alloys.

The only available experimental XMCD spectrum measured at the Pt $N_{6,7}$ edge $(4f \rightarrow 5d)$ is the spectrum of ferromagnetic $CoPt_3$.[34] This spectrum was measured by the total photoelectron yield method. In contrast to the high energy spectra of Pt ($L_{2,3}$, $M_{2,3}$ or $M_{4,5}$ edge), for the ultrasoft x-ray energy region 50 to 80 eV the situation is complicated by the fact that due to small energy difference of Pt $5p$, $4f$, and Co $3p$ core states, six spectra (Pt $O_{2,3}$, Pt $N_{6,7}$, and Co $M_{2,3}$) appear simultaneously in a rather small energy range producing a very complicated spectrum for which interpretation is very difficult without a knowledge of the band structure and corresponding optical matrix elements. It is important to know the correct relative positions of these six spectra. The Dirac-Hartree-Fock-Slater one particle approximation used in this work to calculate the core states is not able to produce a correct energy position of the spectra (due to not taking into account a self-interaction correction, different kinds of relaxation processes and other many-particle effects), therefore we used the experimental XAS (Ref. 34) (see upper panel of Fig. 11) to adjust the energy position of the calculated XMCD spectra. Note that the relative Pt $O_{2,3}-N_{6,7}$ splitting in $CoPt_3$ (Ref. 34) is reported significantly different (about 5 eV) from the corresponding value in pure Pt.[85] Figure 11 shows the theoretically calculated Pt $O_{2,3}$, Pt $N_{6,7}$, and Co $M_{2,3}$ XAS and XMCD spectra in $CoPt_3$ alloy in comparison with the experimental data.[34] There is reasonable agreement with the experimental results for Pt $O_{2,3}$, $N_{6,7}$ and Co M_3 XMCD spectra (all the calculated spectra are presented as separate curves). On the other hand, our one particle calculations were not able to reproduce additional resonance structures at 73 and 76.5 eV which is caused by a strong interference Fano effect.[34] There is also a deviation seen at the Pt $O_{2,3}$ and Co M_2 edge in the sense that the amplitude of the calculated XMCD spectra are too large. An additional peak at a low energy side of the M_3 XMCD spectrum at $\sim$61 eV is also not reproduced by theory.

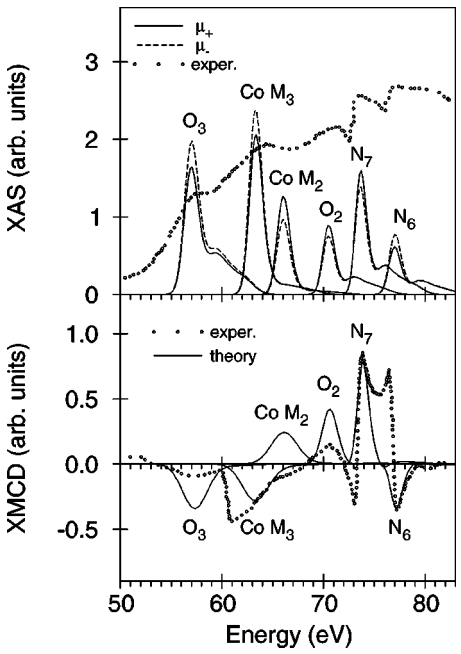

FIG. 11. Theoretically calculated Pt XAS and XMCD spectra at the $O_{2,3}$ and $N_{6,7}$ and Co $O_{2,3}$ edge in $CoPt_3$ compound in comparison with experimental data (Ref. 34).

Finally, we explored the anisotropy of the XMCD spectra with respect to the magnetization direction in these compounds. The influence of the direction of the magnetization on the XMCD spectra was found to be very small in XPt_3 compounds. The comparatively small dependence of the XMCD spectra on the magnetization direction is related to the high degree of isotropy inherent to the Cu_3Au structure.

C. XMCD sum rules

Concurrent with the x-ray magnetic circular dichroism experimental developments, some important magneto-optical

sum rules have been derived in recent years. Thole and van der Laan[86] developed a sum rule relating the integrated signals over the spin-orbit split core edges of the unpolarized XAS to the expectation value of the ground state spin-orbit operator. Later Thole *et al.*[87] and Carra *et al.*[88] derived sum rules to relate the integrated signals over the spin-orbit split core edges of the circular dichroism to ground state orbital and spin magnetic moments by using an ion model for atoms. In the case of solids the corresponding XMCD sum rules were proposed by Ankudinov and Rehr[89] and Guo.[90] Sum rules for x-ray magnetic scattering were derived by Luo *et al.*[91] Recently Benoist *et al.* derived the corrections to the atomic orbital sum rule in solids using orthonormal LMTO's as a single-particle basis for electron band states.[92]

For the $L_{2,3}$ edges the l_z sum rule can be written as

$$\langle l_z\rangle = -n_h \frac{4\int_{L_3+L_2} d\omega(\mu_+ - \mu_-)}{3\int_{L_3+L_2} d\omega(\mu_+ + \mu_-)}, \tag{15}$$

where n_h is the number of holes in the d band $n_h = 10 - n_{3d}$, $\langle l_z\rangle$ is the average of the magnetic quantum number of the orbital angular momentum. The integration is taken over the whole $2p$ absorption region. The s_z sum rule is written as

$$\langle s_z\rangle + \frac{7}{2}\langle t_z\rangle = -n_h \frac{6\int_{L_3} d\omega(\mu_+ - \mu_-) - 4\int_{L_2} d\omega(\mu_+ - \mu_-)}{\int_{L_3+L_2} d\omega(\mu_+ + \mu_-)}, \tag{16}$$

where t_z is the z component of the magnetic dipole operator $\mathbf{t} = \mathbf{s} - 3\mathbf{r}(\mathbf{r}\cdot\mathbf{s})/|\mathbf{r}|^2$ which accounts for the asphericity of the spin moment. It was shown that this term is negligible for cubic systems.[35,57] The integration $\int_{L_3}$ ($\int_{L_2}$) is taken only over the $2p_{3/2}$ ($2p_{1/2}$) absorption region. In these equations, we have replaced the linear polarized spectra, μ_0, by $[\mu_+(\omega) + \mu_-(\omega)]/2$.

Because of the significant implications of the sum rules, numerous experimental and theoretical studies aimed at investigating their validity for itinerant magnetic systems have been reported, but with widely different conclusions. The claimed adequacy of the sum rules varies from very good (within 5% agreement) to very poor (up to 50% discrepancy).[10,87,88,93–98] This lack of a consensus may have several origins. For example, on the theoretical side, it has been demonstrated by circularly polarized $2p$ resonant photoemission measurements of Ni that both the band structure effects and electron-electron correlations are needed to satisfactorily account for the observed MCD spectra.[99] However, it is extremely difficult to include both of them in a single theoretical framework. In addition, the XAS as well as XMCD spectra can be strongly affected (especially for the early transition metals) by the interaction of the excited electron with the created core hole.[100]

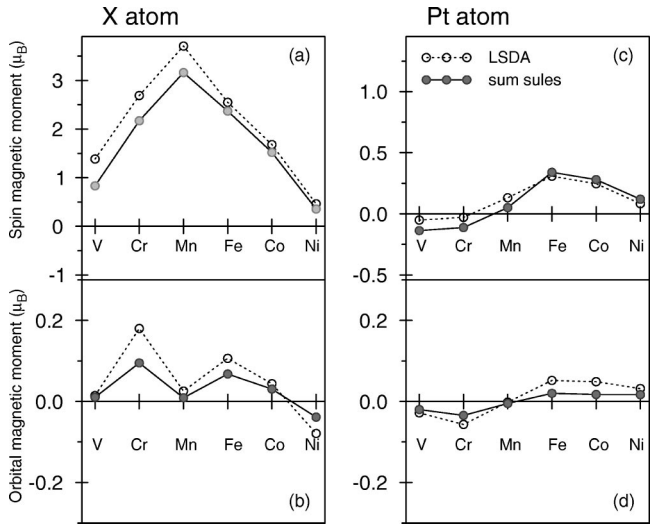

FIG. 12. Theoretically LSDA calculated spin (a),(c) and orbital (b),(d) magnetic moments at the X and Pt sites (open circles) in comparison with estimated data using the sum rules (solid circles) for $X\mathrm{Pt}_3$ and $\mathrm{Fe}_3\mathrm{Pt}$ compounds.

On the experimental side, the indirect x-ray absorption techniques, i.e., the total electron and fluorescence yield methods, are known to suffer from saturation and self-absorption effects that are very difficult to correct for.[95] The total electron yield method can be sensitive to the varying applied magnetic field, changing the electron detecting efficiency or, equivalently, the sample photocurrent. The fluorescence yield method is insensitive to the applied field, but the yield is intrinsically not proportional to the absorption cross section, because the radiative to nonradiative relative core-hole decay probability depends strongly on the symmetry and spin polarization of the XAS final states.[10]

To derive the sum rules a great number of assumptions had to be made.[35] For $L_{2,3}$, they are (1) ignore the exchange splitting for the core levels, (2) replace the interaction operator $\boldsymbol{\alpha}\cdot\mathbf{a}_\lambda$ in Eq. (9) by $\boldsymbol{\nabla}\cdot\mathbf{a}_\lambda$, (3) ignore the asphericity of the core states, (4) ignore $p\rightarrow s$ transitions, (5) ignore the difference of $d_{3/2}$ and $d_{5/2}$ radial wave functions, and (6) ignore the interatomic hybridization, which is reflected on the nontreatment of any energy dependence of the radial matrix elements. The three last points are the most important. The problem of the ignoring of the $p\rightarrow s$ transitions was considered by Wu and Freeman[98] in the case of pure Fe, Co, Ni and their surfaces. They demonstrate that the application of the spin sum rule results in an error up to 52% for the Ni(001) surface. On the other hand, the orbital sum rule is affected much less.

Taking into account all the above mentioned problems it is interesting to compare the spin and orbital magnetic moments obtained from the theoretically calculated XAS and XMCD spectra through the sum rules [Eqs. (15),(16)] with directly calculated LSDA values. In this case we at least avoid all the experimental problems.

Figure 12 shows direct and sum rule derived spin and orbital magnetic moments from the theoretical XMCD $L_{2,3}$

spectra. The number of the $3d$ and Pt $5d$ electrons is calculated by integrating the element and lj projected density of states inside each atomic sphere. The values $n_{3d}=$ 3.644, 4.614, 5.606, 6.567, 7,776, 8.854 and $n_{5d}=$ 8.302, 8.187, 8.213, 8.136, 8.138, 8.134 for VPt_3, $CrPt_3$, $MnPt_3$, Fe_3Pt, $CoPt_3$, and $NiPt_3$, respectively.

As can be seen from Fig. 12, the general trend of the sum rule results is in a good agreement with the LSDA calculated spin and orbital magnetic moments for both the X and Pt sites. The orbital magnetic moments at X and Pt sites agree well with the direct calculations, but the spin magnetic moments deduced from the theoretical MXCD spectra are underestimated for VPt_3, $CrPt_3$, and $MnPt_3$ for both the transition metal and Pt sites. The disagreement at X sites reaches the 40% in VPt_3 and reduces to 19% in $CrPt_3$, 15% in $MnPt_3$ and becomes less than 10% in Fe_3Pt, $CoPt_3$, and $NiPt_3$ compounds. Such behavior arises because the sum rules ignore the p to s transitions which play an essential role in the formation of the spin magnetic moments in early transition metals. In Fe, Co, and Ni the relative contribution of the s states is reduced and the effect plays a minor role. Thus, first principles determinations of both the XMCD spectra and ground state properties (M_l and M_s) are probably required for quantitative interpretation of the experimental results.

IV. SUMMARY

We have studied by means of an *ab initio* fully relativistic spin-polarized Dirac linear muffin-tin orbital (LMTO) method the electronic structure and the x-ray magnetic circular dichroism for nine transition-metal-platinum alloys with Cu_3Au-type crystal structure in the local spin-density approximation.

The orbital and spin magnetic moments of the Cu_3Au-type transition metal intermetallics XPt_3, $X=$ V, Cr, Mn, Fe, Co, Ni and X_3Pt ($X=$ Fe, Co, Ni) have been evaluated from first-principles electronic structure calculations. The obtained moments are in good agreement with neutron and XMCD experimental data. The variation seen in the $3d$ metal and Pt magnetic moments can be understood by analyzing the spin-projected DOS's and site- and l-projected density of the expectation value of $\hat{l}_z$ $[dm_{tl}(E)]$ and their integrated values $[m_{tl}(E)]$. It was found that the hybridization between the $3d$ metal and Pt d states plays an important role in determining the variation.

We demonstrated that XMCD K spectrum reflects the orbital polarization in differential form of the p states [the $dml_{l=1}(E)$ function]. Due to small exchange splitting of the initial $1s$-core states only the exchange and spin-orbit splitting of the final $4p$ states is responsible for the observed dichroism at the K edge.

The XMCD spectra of transition metals for the $L_{2,3}$ edge are mostly determined by the strength of the SO coupling of the initial $2p$ core states and spin-polarization of the final empty $3d_{3/2,5/2}$ states while the exchange splitting of the $2p$ core states as well as SO coupling of the $3d$ valence states are of minor importance. The theoretically calculated $L_{2,3}$ XMCD spectra are in a good agreement with the experimental measurements. The spectra for Fe_3Pt, $CoPt_3$, and $NiPt_3$ are very similar with a strong decreasing of the dichroic signal in $NiPt_3$ reflecting the decrease of the spin magnetic moment and also the lack of unoccupied $3d$ states.

We found a rather pronounced XMCD at the Pt $L_{2,3}$ edge. In ferromagnetic compounds $MnPt_3$, Fe_3Pt, and $CoPt_3$, the XMCD spectrum was found to be negative at L_3 and positive at L_2 edges. The XMCD in $MnPt_3$ at the L_3 and L_2 edges are of nearly equal magnitude, which suggest that the orbital magnetic moment almost vanishes in the Pt $5d$ states in this compound. In ferrimagnetically ordered VPt_3 and $CrPt_3$ the XMCD spectra at the L_3 edge are positive with a double peak structure, in a good agreement with the experimental measurements.

Due to the dipole selection rules the N_6 absorption spectra resemble the L_3 and O_3 spectra, whereas the N_7 spectrum is the analog of the L_2 and O_2 ones. Because of the relatively small spin-orbit splitting of the $4f$ states of Pt ($\sim$3.3 eV), the N_6 and the N_7 spectra have an appreciable overlap.

Due to the small energy differences of Pt $5p$, $4f$ and Co $3p$ core states, six spectra (Pt $O_{2,3}$, Pt $N_{6,7}$, and Co $M_{2,3}$) appear simultaneously in a rather small energy range producing a very complicated spectrum. We found reasonable agreement with the experimental results for Pt $O_{2,3}$, $N_{6,7}$ and Co M_3 XMCD spectra in $CoPt_3$. On the other hand, our one particle calculations were not able to reproduce additional resonance structures at 73 and 76.5 eV which are caused by a strong interference Fano effect.[34]

The recently derived sum rules for the orbital and spin magnetic moments were tested for these compounds. The orbital magnetic moments at X and Pt sites obtained from the sum rules agree with the direct calculations, whereas the spin moments at both the transition metal and Pt sites are somewhat underestimated in VPt_3, $CrPt_3$, and $MnPt_3$ due to the neglect of $p \rightarrow s$ transitions in the sum rules.

ACKNOWLEDGMENTS

This work was carried out at the Ames Laboratory, which is operated for the U.S. Department of Energy by Iowa State University under Contract No. W-7405-82. This work was supported by the Director for Energy Research, Office of Basic Energy Sciences of the U.S. Department of Energy. V.N. Antonov gratefully acknowledges the hospitality during his stay at Ames Laboratory.

*Permanent address: Institute of Metal Physics, 36 Vernadskii Street, 03142 Kiev, Ukraine.

[1] A short modern history of XMD can be found at URL http://psi–k.dl.ac.uk/psi–k/hp.html

[2] J.L. Erskine and E.A. Stern, Phys. Rev. B **12**, 5016 (1975).

[3] B.T. Thole, G. van der Laan, and G.A. Sawatzky, Phys. Rev. Lett. **55**, 2086 (1985).

[4] G. van der Laan, B.T. Thole, G.A. Sawatzky, J.B. Goedkoop, J.C. Fuggle, J.M. Esteva, R.C. Karnatak, J.P. Remeika, and H.A. Dabkowska, Phys. Rev. B **34**, 6529 (1986).

[5] G. Schütz, W. Wagner, W. Wilhelm, P. Kienle, R. Zeller, R. Frahm, and G. Materlik, Phys. Rev. Lett. **58**, 737 (1987).
[6] G. Schütz, R. Frahm, P. Mautner, R. Wienke, W. Wagner, W. Wilhelm, and P. Kienle, Phys. Rev. Lett. **62**, 2620 (1989).
[7] H. Ebert, P. Strange, and B.L. Gyorffy, J. Appl. Phys. **63**, 3055 (1988).
[8] C.T. Chen, F. Sette, Y. Ma, and S. Modesti, Phys. Rev. B **42**, 7262 (1990).
[9] G. van der Laan and B.T. Thole, Phys. Rev. B **43**, 13 401 (1991).
[10] C.T. Chen, Y.U. Idzerda, H.-J. Lin, N.V. Smith, G. Meigs, E. Chaban, G.H. Ho, E. Pellegrin, and F. Sette, Phys. Rev. Lett. **75**, 152 (1995).
[11] C.M. Schneider, K. Holldack, M. Kinzler, M. Grunze, H.P. Oepen, F. Schäfers, H. Petersen, K. Meinel, and J. Kirschner, Appl. Phys. Lett. **63**, 2432 (1993).
[12] K. Holldack, F. Schäfers, T. Kachel, and J. Packe, Rev. Sci. Instrum. **67**, 2485 (1996).
[13] J.J.M. Franse and R. Gersdorf, in *Magnetic Properties of Metals-3d, 4d and 5d Elements, Alloys and Compounds*, Landolt-Börnstein, New Series, Vol. 19a, edited by H.P.J. Wijn (Springer-Verlag, Berlin, 1986).
[14] J.G. Booth, in *Ferromagnetic Materials*, edited by E.P. Wohlfarth and K.H.J. Buschow (North-Holland, Amsterdam, 1988), Vol. 4.
[15] B. Antonini, F. Lucari, F. Menzinger, and A. Paoletti, Phys. Rev. **187**, 611 (1969).
[16] Y. Itoh, T. Sasaki, and T. Mizoguchi, Solid State Commun. **15**, 807 (1974).
[17] F. Menzinger and A. Paoletti, Phys. Rev. **143**, 365 (1966).
[18] S. Imada, T. Muro, T. Shishidou, S. Suga, H. Maruyama, K. Kobayashi, H. Yamazaki, and T. Kanomata, Phys. Rev. B **59**, 8752 (1999).
[19] J. Kübler, J. Magn. Magn. Mater. **45**, 415 (1984).
[20] M. Podgorny, Phys. Rev. B **43**, 11 300 (1991).
[21] A. Hasegawa, J. Phys. Soc. Jpn. **54**, 1477 (1985).
[22] T. Tohyama, Y. Ohta, and M. Shimizu, J. Phys.: Condens. Matter **1**, 1789 (1989).
[23] T. Suda, M. Shirai, and K. Motizuki, Int. J. Mod. Phys. B **7**, 765 (1993).
[24] M. Shirai, H. Maeshima, and N. Suzuki, J. Magn. Magn. Mater. **140-144**, 105 (1995).
[25] G. Stajer, C.J. Yahnker, D.R. Haeffner, D.M. Mills, L. Assoufid, B.N. Harmon, and Z. Zuo, J. Phys.: Condens. Matter **11**, L253 (1999).
[26] K. Iwashita, T. Oguchi, and T. Jo, Phys. Rev. B **54**, 1159 (1996).
[27] P. Oppeneer, T. Kraft, V.N. Antonov, H. Eschrig, A.Ya. Perlov, and A.N. Yaresko, J. Phys.: Condens. Matter **8**, 5769 (1996).
[28] E.T. Kulatov, Yu.A. Uspenskii, and S.V. Halilov, J. Magn. Magn. Mater. **163**, 331 (1996).
[29] S. Uba, L. Uba, A.N. Yaresko, A.Ya. Perlov, V.N. Antonov, and R. Gontarz, Phys. Rev. B **53**, 6526 (1996).
[30] H. Maruyama, F. Matsuoka, K. Kobayashi, and H. Yamazaki, Physica B **208-209**, 787 (1995).
[31] H. Maruyama, F. Matsuoka, K. Kobayashi, and H. Yamazaki, J. Magn. Magn. Mater. **140-144**, Part 1, 43 (1995).
[32] E.E. Alp, M. Ramanathan, S. Salem-Sugui, Jr., F. Oliver, V. Stojanoff, and D.P. Siddond, Rev. Sci. Instrum. **63**, 1221 (1992).
[33] W. Grange, M. Maret, L.-P. Kappler, J. Vogel, A. Frontaine, F. Petroff, G. Krill, A. Rogalev, J. Goulon, M. Finazzi, and N.B. Brookes, Phys. Rev. B **58**, 6298 (1998).
[34] T. Shishidou, S. Imada, T. Muro, F. Oda, A. Kimura, S. Suga, T. Miyahara, T. Kanomata, and T. Kaneko, Phys. Rev. B **55**, 3749 (1997).
[35] H. Ebert, Rep. Prog. Phys. **59**, 1665 (1996).
[36] J.P. Hannon, G.T. Trammel, M. Blume, and D. Gibbs, Phys. Rev. Lett. **61**, 1245 (1988).
[37] S.W. Lovsey and S.P. Collins, *X-Ray Scattering and Absorption in Magnetic Materials* (Oxford University Press, Oxford, 1996).
[38] J.B. Kortight and S.-K. Kim, Phys. Rev. B **62**, 12 216 (2000).
[39] H. Friezer, IEEE Trans. Magn. **4**, 152 (1968).
[40] G.Y. Guo, Phys. Rev. B **55**, 11 619 (1998).
[41] P.N. Argyres, Phys. Rev. **97**, 334 (1955).
[42] P.J. Durham, in *The Electronic Structure of Complex Systems*, edited by P. Phariseu and W.M. Temmerman (Plenum, New York, 1984).
[43] W.H. Kleiner, Phys. Rev. **142**, 318 (1966).
[44] F.U. Hillebrecht, C. Roth, H.B. Rose, W.G. Park, E. Kisker, and N.A. Cherepkov, Phys. Rev. B **53**, 12 182 (1996).
[45] J. G. Menchero, Phys. Rev. B **57**, 993 (1998).
[46] G. van der Laan, J. Magn. Magn. Mater. **148**, 53 (1995).
[47] G. van der Laan, J. Electron Spectrosc. Relat. Phenom. **86**, 41 (1997).
[48] G. van der Laan, J. Phys.: Condens. Matter **9**, L259 (1997).
[49] G. van der Laan, Phys. Rev. B **57**, 5250 (1998).
[50] J.G. Menchero, Phys. Rev. B **57**, 1001 (1998).
[51] A. Fanelsa, R. Schellenberg, F.U. Hillebrecht, E. Kisker, J.G. Menchero, A.P. Kaduwela, C.S. Fadley, and M.A. Van Hove, Phys. Rev. B **54**, 17 962 (1996).
[52] J. G. Menchero, C.S. Fadley, G. Panaccione, F. Sirotti, and G. Ross, Solid State Commun. **103**, 197 (1997); J. Henk and R. Feder, Phys. Rev. B **55**, 11 476 (1997).
[53] J.G. Menchero, Phys. Rev. B **55**, 5505 (1997).
[54] R. Schellenberg, E. Kisker, A. Fanelsa, F.U. Hillebrecht, J.G. Menchero, A.P. Kaduwela, C.S. Fadley, and M.A.V. Hove, Phys. Rev. B **57**, 14 310 (1998).
[55] H. Ebert, L. Baumgarten, C.M. Schneider, and J. Kirschner, Phys. Rev. B **44**, 4406 (1991).
[56] H. Ebert and G.-Y. Guo, J. Magn. Magn. Mater. **148**, 178 (1995).
[57] G.Y. Guo, H. Ebert, W.M. Temmerman, and P.J. Durham, Phys. Rev. B **50**, 3861 (1994).
[58] E. Tamura, G.D. Waddill, J.G. Tobin, and P.A. Sterne, Phys. Rev. Lett. **73**, 1533 (1994).
[59] A.H. MacDonald and S.H. Vosko, J. Phys. C **12**, 2977 (1979).
[60] O.K. Andersen, Phys. Rev. B **12**, 3060 (1977).
[61] D.D. Koelling and B.N. Harmon, J. Phys. C **10**, 3107 (1977).
[62] V.V. Nemoshkalenko, A.E. Krasovskii, V.N. Antonov, Vl.N. Antonov, U. Fleck, H. Wonn, and P. Ziesche, Phys. Status Solidi B **120**, 283 (1983).
[63] H. Ebert, Phys. Rev. B **38**, 9390 (1988).
[64] I.V. Solovyev, A.B. Shik, V.P. Antropov, A.I. Liechtenstein, V.A. Gubanov, and O.K. Andersen, Sov. Phys. Solid State **31**, 1285 (1989).
[65] V.N. Antonov, A.Ya. Perlov, A.P. Shpak, and A.N. Yaresko, J. Magn. Magn. Mater. **146**, 205 (1995).
[66] H. Ebert, H. Freyer, A. Vernes, and G.-Y. Guo, Phys. Rev. B **53**, 7721 (1996).
[67] V.N. Antonov, A.I. Bagljuk, A.Ya. Perlov, V.V. Nemoshkalenko, Vl.N. Antonov, O.K. Andersen, and O. Jepsen, Fiz. Nizk. Temp. **19**, 689 (1993) [Low Temp. Phys. **19**, 494 (1993)].

[68] V.V. Nemoshkalenko, V.N. Antonov, Vl.N. Antonov, W. John, H. Wonn, and P. Ziesche, Phys. Status Solidi B **111**, 11 (1982); V.V. Nemoshkalenko, V.N. Antonov, Vl.N. Antonov, and W. John, *ibid.* **93**, 575 (1979).
[69] V.N. Antonov, V.P. Antropov, B.N. Harmon, A.N. Yaresko, and A.Ya. Perlov, Phys. Rev. B **59**, 14 552 (1999).
[70] U. von Barth and L. A. Hedin, J. Phys. C **5**, 1629 (1972).
[71] V.V. Nemoshkalenko and V.N. Antonov, *Computational Methods in Solid State Physics* (Gordon and Breach, London, 1998).
[72] P.E. Blöchl, O. Jepsen, and O.K. Andersen, Phys. Rev. B **49**, 16 223 (1994).
[73] J.C. Fuggle and J.E. Inglesfield, *Unoccupied Electronic States. Topics in Applied Physics* (Springer, New York, 1992), Vol. 69.
[74] J.E. Müller, O. Jepsen, and J.W. Wilkins, Solid State Commun. **42**, 365 (1982).
[75] P. Villars and L.D. Calvert, *Pearson's Handbook of Crystallographic Data for Intermetallic Phases* (ASM International, Materials Park, 1991).
[76] J.S Booth, in *Ferromagnetic Materials*, edited by E.P. Wohlfarth and K.H.J. Buschow (North-Holland, Amsterdam, 1988), Vol. 4.
[77] M.B. Stern, in *Magnetic Properties of Metals*, edited by H.P.J. Wijn, Landolt-Börnstein, New Series, Group III, Vol. 19, Pt. a (Springer-Verlag, Berlin, 1986).
[78] L. Uba, S. Uba, V.N. Antonov, T. Ślęzak, J. Korecki, and A.N. Yaresko, Phys. Rev. B **62**, 13 731 (2000).
[79] J.H. van Vleck *Electric and Magnetic Susceptibilities* (Oxford University Press, Oxford, 1932).
[80] P. Carra, B.N. Harmon, B.T. Thole, M. Altarelli, and G.A. Sawatzky, Phys. Rev. Lett. **66**, 2495 (1991).
[81] H. Ebert, J. Phys.: Condens. Matter **1**, 9111 (1989).
[82] H.J. Gotsis and P. Strange, J. Phys.: Condens. Matter **6**, 1409 (1994).
[83] M.S.S. Brooks and B. Johansson, in *Spin-Orbit Influenced Spectroscopies*, edited by H. Ebert and G. Schultz (Springer, Heidelberg, 1996), p. 211.
[84] J. Igarashi and K. Hirai, Phys. Rev. B **50**, 17 820 (1994).
[85] See URL http://www.webelements.com
[86] G. van der Laan and B.T. Thole, Phys. Rev. B **38**, 3158 (1988).
[87] B.T. Thole, P. Carra, F. Sette, and G. van der Laan, Phys. Rev. Lett. **68**, 1943 (1992); G. van der Laan and B.T. Thole, Phys. Rev. B **53**, 14 458 (1996); G. van der Laan, *ibid.* **57**, 112 (1998).
[88] P. Carra, B.T. Thole, M. Altarelli, and X. Wang, Phys. Rev. Lett. **70**, 694 (1993).
[89] A. Ankudinov and J.J. Rehr, Phys. Rev. B **51**, 1282 (1995).
[90] G.Y. Guo, Phys. Rev. B **57**, 10 295 (1998).
[91] J. Luo, G.T. Trammell, and J.P. Hannon, Phys. Rev. Lett. **71**, 287 (1993).
[92] R. Benoist, P. Carra, and O.K Andersen, Phys. Rev. Lett. (to be published).
[93] Y. Wu, J. Stöhr, B.D. Hermsmeier, M.G. Sumant, and D. Weller, Phys. Rev. Lett. **69**, 2307 (1992).
[94] J. Vogel and M. Sacchi, Phys. Rev. B **49**, 3230 (1994).
[95] T. Böske, W. Clemens, C. Carbone, and W. Eberhardt, Phys. Rev. B **49**, 3230 (1994).
[96] W.L. O'Brain, B.P. Tonner, G.R. Harp, and S.S.P. Parkin, J. Appl. Phys. **76**, 6462 (1994); W.L. O'Brain and B.P. Tonner, Phys. Rev. B **50**, 12 672 (1994).
[97] G.Y. Guo, H. Ebert, W.M. Temmerman, and P.J. Durham, in *Metallic Alloys: Experimental and Theoretical Perspectives*, Vol. 256 of *NATO Advanced Studies Institute, Series E: Applied Sciences*, edited by J.S. Faulkner and R.G. Jordan (Kluwer Academic, Dordrecht, 1994), pp. 339–348.
[98] R. Wu and A.J. Freeman, Phys. Rev. Lett. **73**, 1994 (1994).
[99] L.H. Tjeng *et al.*, Phys. Rev. B **48**, 13 378 (1994).
[100] J. Zaanen, G.A. Sawatzky, J. Fink, W. Speier, and J.C. Fuggle, Phys. Rev. B **32**, 4905 (1985); J. Schwitalla and H. Ebert, Phys. Rev. Lett. **80**, 4586 (1998).